A Study of the Charged Current Trigger Efficiency for the ZEUS Detector

Alex Tapper
Imperial College

June 26, 1998

Abstract

The charged current trigger efficiency for the ZEUS detector has been evaluated using $10.7pb^{-1}$ of data taken in 1996 and $26.5pb^{-1}$ taken in 1997. The efficiencies are compared with Monte Carlo simulation. Low Q^2 neutral current events are used as a low bias sample to study the trigger and the efficiency is calculated relative to a a sample of charged current events selected offline. The trigger efficiency is found to be 98.75 ± 0.70 % for 1996 data, and 99.14 ± 0.37 % for 1997 data. The difference in trigger efficiency between data and Monte Carlo is found to be $< 1\%$.

Contents

1 Introduction

The charged current cross-section for e^+p deep inelastic scattering (DIS) reactions is measured at high Q^2 using the ZEUS detector. The cross-section is given by:

$$\sigma_{cc} = \frac{N_{evts}}{A \cdot L} \quad (1)$$

where N_{evts} is the number of events observed, L is the integrated luminosity of the data sample, and A is the detector acceptance. The detector acceptance is calculated from a Monte Carlo simulation of the reaction and the detector. The motivation for evaluating the charged current trigger efficiency is that any discrepancy in the Monte Carlo simulation of the trigger will effect the cross-section measurment directly, through the detector acceptance A. So in order to make an accurate measurment of the cross-section it is vital that the trigger efficiency is well simulated in the Monte Carlo.

The method chosen to evaluate the trigger efficiency uses low Q^2 neutral current events, as a low bias sample, to determine the characteristics of the trigger. The efficiency is then calculated compared to a charged current event sample selected offline. Only the first level trigger (see section 6) is considered.

2 The ZEUS detector

The ZEUS detector [1] is used to study positron(electron)-proton (ep) interactions in the HERA [2] collider. At HERA positrons of energy 27.5 GeV are collided with protons of energy 820 GeV, to give ep interactions at a centre of mass energy of $\sqrt{s} = 300$ GeV. Figure 1 shows the layout of the ZEUS dector. The ZEUS coordinate system is right-handed with the Z axis pointing in the proton direction, (referred to as forward) and the X axis horizontal, pointing towards the centre of HERA. The main components of the detector used in this analysis are the central tracking detector (CTD), and the uranium calorimeter.

The CTD is a cylindrical drift chamber, positioned at the centre of the ZEUS detector, and enclosed in a solenoidal magnetic field of 1.43 T. It is used to measure the momentum of charged particles emerging from the collisions. The CTD covers the range $15^\circ < \theta < 164^\circ$, and consists of 72 radial layers, organised into 9 superlayers. Each superlayer has wires either parallel to the beam line, or inclined at $\pm 5^\circ$, in order to determine the z-position of tracks. For trigger purposes 3 of the superlayers determine the z-position of tracks from timing information. Typical resolution in $r - \phi$ is $190\mu m$, which gives a transverse momentum resolution of $0.005 P_T \oplus 0.0016$ (with P_T in GeV). For charged current events the z position resolution for the interaction vertex is ~ 1.1 cm. For neutral current events the presence of a scattered positron track improves the resolution of the z position of the interaction vertex to ~ 0.15 cm.

The calorimeter is split into three sections, forward (FCAL), barrel (BCAL), and rear (RCAL). The calorimeter is hermetic apart from holes in FCAL and RCAL for the beam pipe, and covers 99.7% of the solid angle around the interaction point. Each section of the calorimeter is divided into electromagnetic (EMC) cells, and hadronic (HAC) cells. FCAL and BCAL have two layers of HAC cells and one layer of EMC cells. RCAL has one layer of each of EMC and HAC cells. The cells are made up of sheets of depleted uranium absorber, interleaved with sheets of plastic scintillator. Light from the scintillator material is conveyed to two photomultiplier tubes (PMTs), on either side of each cell, where is is converted into an electrical signal. The energy resolution of the calorimeter from test beam data is $35\%/\sqrt{E} \oplus 2\%$ for hadronic deposits and $18\%/\sqrt{E} \oplus 1\%$ for electromagnetic energy (with E in GeV). The calorimeter also provides timing information for energy deposits. The resolution of this timing is better than 1 ns, for energy deposits greater than 4.5 GeV.

3 Kinematics

The kinematics of the charged current and neutral current DIS processes (see figure 2) are defined by the four-momenta of the incoming positron (k), the incoming proton (P), the outgoing lepton (k') and the final hadronic state (P'). The four-momentum transfer between the positron and the proton is given by $q = k - k' = P - P'$. The square of the energy in the ep centre of mass is given by $s = (k + P)^2$. Three Lorentz invariant quantities are usually defined in terms of the four-momenta k, P and q:

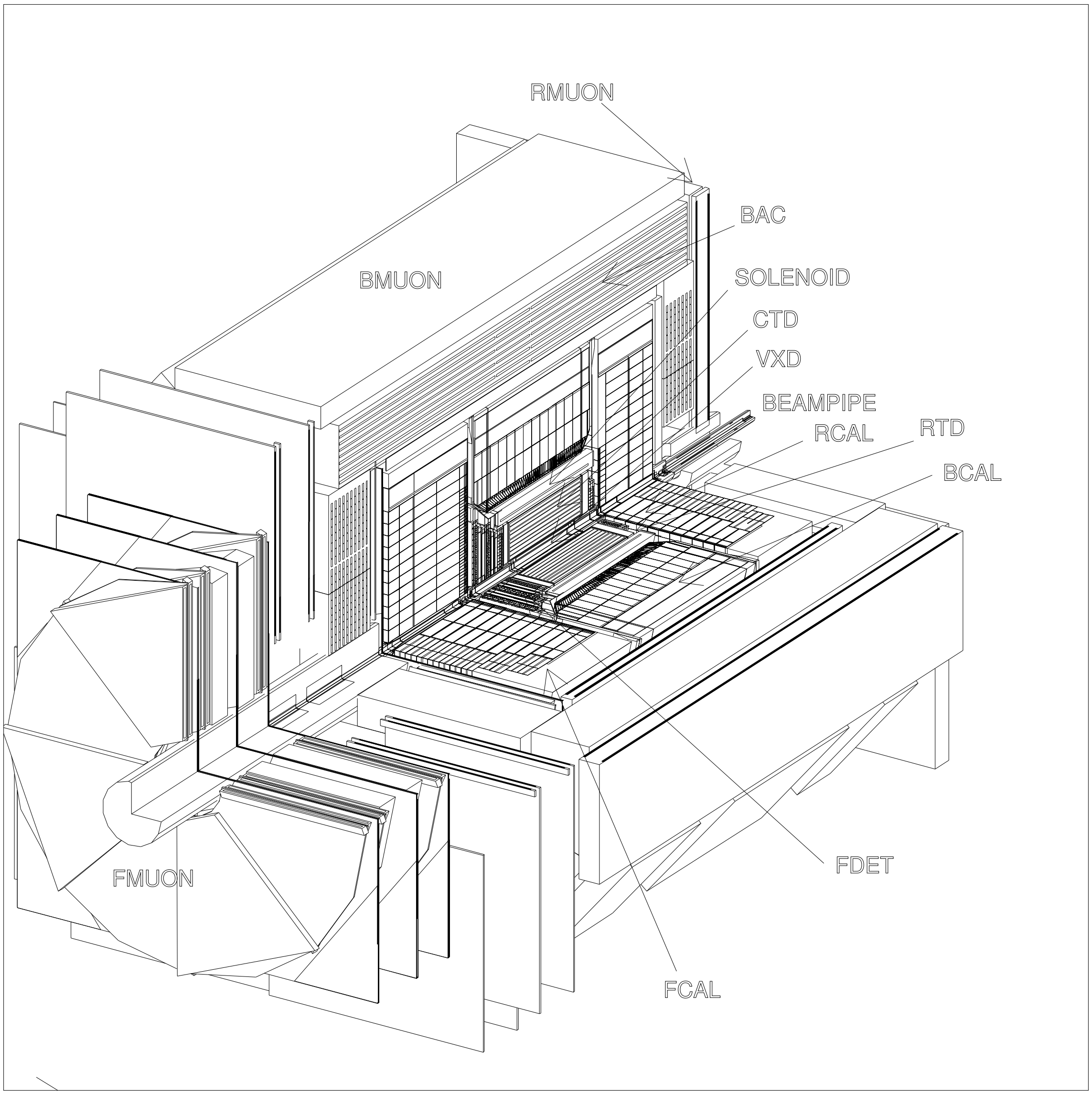

Figure 1: A cut-away view of the ZEUS detector.

- $Q^2 = -q^2$, the negative square of the four-momentum transfer,
- $x = \frac{Q^2}{2p \cdot q}$, the Bjorken scaling variable,
- $y = \frac{q \cdot P}{k \cdot P}$, the fractional energy transfer to the proton in its rest frame.

These variables are related by $Q^2 = xys$, when the masses of the particles can be neglected. At any given value of s, the kinematic variables x, y and Q^2 can be reconstructed from any two of the four measured quantities shown in figure 3: E'_e, θ_e, E_X, and γ.

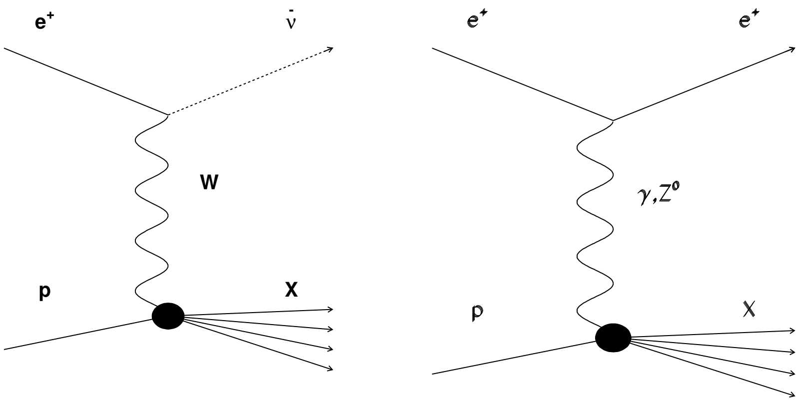

Figure 2: Feynman diagrams for charged current (left) and neutral current (right) DIS.

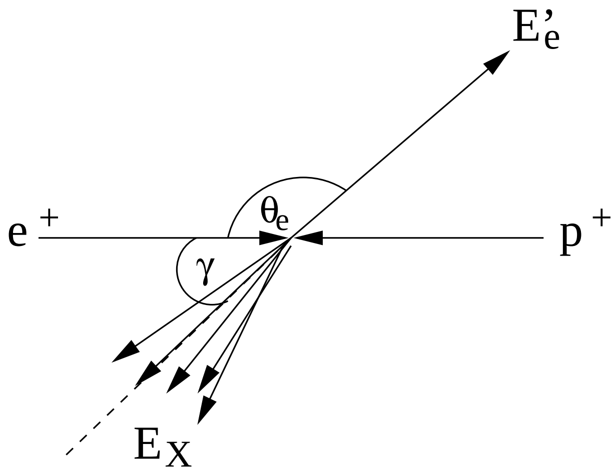

Figure 3: Kinematics of neutral current DIS, showing the scattered positron, with energy E'_e and angle θ_e, and the hadronic jet, with energy E_X and angle γ.

3.1 Jacquet-Blondel reconstruction

The Jacquet-Blondel [3] method must be used to reconstruct the kinematic variables for the charged current event sample, because the outgoing lepton is a neutrino, which is not detected. The missing transverse momentum,

$$P_t = \sqrt{\left(\sum_i p_X^i\right)^2 + \left(\sum_i p_Y^i\right)^2} \tag{2}$$

and the quantity δ,

$$\delta = \sum_i (E^i - p_Z^i) \tag{3}$$

are used, where the sums run over all calorimeter cells and p^i are the momenta assigned to each cell. These momenta are calculated by projecting the energy deposited onto the x, y and z axis assuming zero mass and using the measured vertex position. The Jacquet-Blondel estimators of y, x and Q^2 are given by

$$y_{JB} = \frac{\delta}{2E_e} \tag{4}$$

$$x_{JB} = \frac{P_t^2}{s y_{JB}(1 - y_{JB})} \tag{5}$$

$$Q_{JB}^2 = \frac{P_t^2}{1 - y_{JB}} \tag{6}$$

where E_e is the positron beam energy.

3.2 Electron method of reconstruction

The electron method of reconstruction [4] was used for the neutral current event sample. The kinematic variables x, y and Q^2 are calculated from the scattered positron energy E_e' and angle θ_e using the equations:

$$x_e = \frac{E_e}{E_p} \frac{E_e'(1 + cos\theta_e)}{2E_e - E_e'(1 - cos\theta_e)} \tag{7}$$

$$y_e = 1 - \frac{E_e'}{2E_e}(1 - cos\theta_e) \tag{8}$$

$$Q_e^2 = s x_e y_e \tag{9}$$

4 Monte Carlo samples

The Monte Carlo (MC) events used were generated with DJANGO [5], which is an interface between the LEPTO [6] and HERACLES [7] generators. LEPTO simulates the hard scattering process and HERACLES provides single loop electroweak corrections and initial state radiation from the incoming positron. Also HERACLES provides final state radiation for the neutral current events.

Four samples of charged current DIS Monte Carlo were used with different minimum Q^2 cuts at generator level. Using separate samples in this way eliminates the need to generate large numbers of low Q^2 events in order to cover the HERA Q^2 range. The samples are then combined using weighting appropriate to the luminosity of each sample. Two samples of neutral current DIS Monte Carlo were used. The Q^2 thresholds and luminosities of the samples used are detailed in table 1.

MC sample	No. of events	Cross-section	Luminosity
CC $Q^2 > 10$ GeV^2	19888	39.71 pb	501 pb^{-1}
CC $Q^2 > 5000$ GeV^2	19756	2.416 pb	8177 pb^{-1}
CC $Q^2 > 10000$ GeV^2	19904	0.4461 pb	446.8 pb^{-1}
CC $Q^2 > 20000$ GeV^2	19947	0.02867 pb	695744 pb^{-1}
NC $Q^2 > 4$ GeV^2	238415	307.40 nb	775.6 nb^{-1}
NC $Q^2 > 100$ GeV^2	139186	7.582 nb	18.36 pb^{-1}

Table 1: Summary of MC samples used.

5 Event selection

The charged current and neutral current samples are selected from the $10.7pb^{-1}$ of data taken in 1996 and the $26.5pb^{-1}$ taken in 1997. All plots in this section show the number of events normalised to $1pb^{-1}$.

5.1 Backgrounds

Background events to the charged current and neutral current DIS signals can be split into two catagories, *ep* interactions and non-*ep* interactions. The main sources of background events are listed below:

5.1.1 Non-*ep* background events

- Beam-gas events, where the proton or positron beam interacts with residual gas in the beam pipe. Typically these events have high track multiplicity and high activity in the calorimeter.
- Cosmic muon events, where muons produced in the upper atmosphere penetrate the detector.
- Halo muon events, where muons are produced upstream of the detector by interactions between one of the particle beams and some part of the accelerator. These muons travel through the detector parallel to the beampipe.

5.1.2 *ep* background events

- Photo-production events, where Q^2 is close to zero, can have missing P_T because the scattered positron is lost down the RCAL beam pipe or in a crack between calorimeter sections, and is not detected. Also hadronic deposits can be mis-identified as electons. So photo-production events contribute as background to charged current and neutral current DIS events.
- Poorly measured neutral current DIS events can have missing P_T and are therefore a background to charged current DIS events.

5.2 Charged current Sample

- $-50cm < Z_{vtx} < 50cm$
  The z position of the *ep* interaction vertex, measured by the CTD, is required to be within 50cm of the nominal interaction point at z=0 (see figure 4). Confining the vertex to the central region of the detector helps to reject non-ep interactions. Good agreement is observed between data and MC in the central peak region. There is some discrepancy between 1997 data and MC in the outer regions of the distribution.
- $N_{vtx} \geq 1$
  where N_{vtx} is the number of vertex tracks. A vertex track is defined as a track with P_T >0.2 GeV which passes within 1.5cm of the nominal beam line. Requiring at least one vertex track reduces background from non-*ep* interactions (see figure 5).
- $N_{vtx} > 0.25(N_{trks}\text{-}20)$
  where N_{trks} is the number of particle tracks. A large fraction of tracks are required to be vertex tracks. The number of beam-gas background events is reduced since beam-gas events are characterised by a large number of non-vertex tracks.
- P_T >10 GeV
  Net transverse momentum, P_T, due to the momentum of the undetected neutrino, is the primary characteristic of charged current *ep* events (see figure 6).
- P_{TEXIR} >9 GeV
  where P_{TEXIR} is the transverse momentum evaluated excluding the cells adjacent to the forward beam pipe. This cut removes beam-gas events which deposit energy at large angles (see figure 6).
- P_T/E_T >0.4 for $P_T > 20$ GeV
  P_T/E_T >0.5 for $P_T < 20$ GeV
  where the total transverse energy, E_T, is defined as:

$$E_T = \sum_i \sqrt{(p_X^i)^2 + (p_X^i)^2}$$

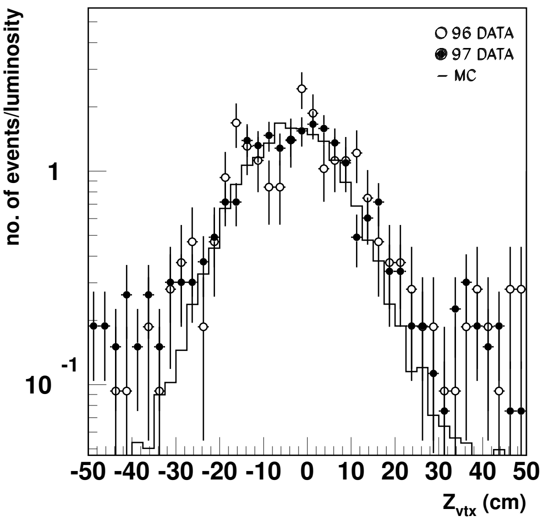

Figure 4: Distribution of the z position of the interaction vertex, for the charged current event sample after all cuts have been applied.

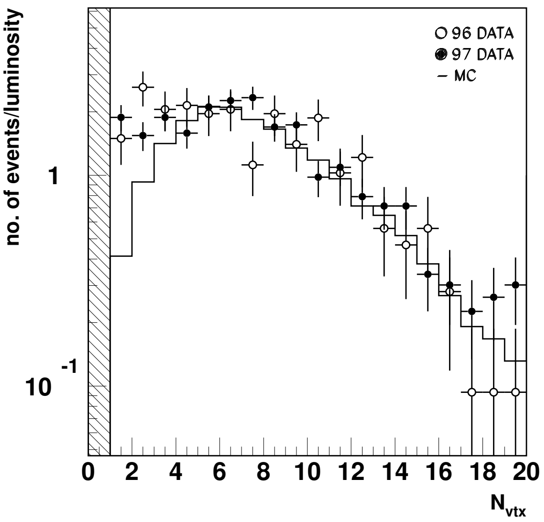

Figure 5: Distribution of vertex track multiplicity, for the charged current event sample after all other cuts have been applied. The shaded area shows those events that pass all other cuts but are rejected by the vertex track multiplicity cut. In the unshaded region there is generally good agreement apart from an excess of data events in the first two bins.

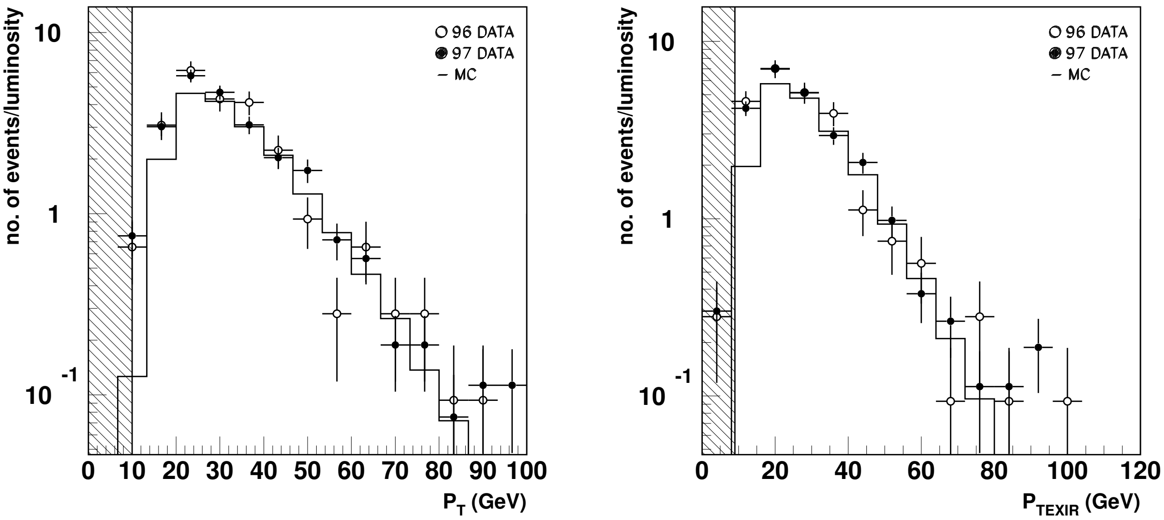

Figure 6: Distributions for total P_T (left), and P_T excluding the inner ring of cells in FCAL (right), after all other cuts have been applied. The shaded areas shows those events that pass all other cuts but are rejected by the P_T or P_{TEXIR} cut. In the unshaded regions there is generally good agreement apart from a small excess of data events at low P_T.

where the sums run over all calorimeter cells. The quantity P_T/E_T characterises how collimated the transverse energy flow is. Requiring a highly collimated, or single jet-like event reduces backgound from beam-gas interactions and photo-production (see figure 7).

- E_{BHAC}/E_B <0.9
  where E_{BHAC} is the energy measured by the HAC cells in BCAL, and E_B is the total energy measured in BCAL. This cut requires that the energy deposited in BCAL must not be entirely hadronic. Halo muons and cosmic rays which miss the EMC layer, but pass through the HAC cells are removed (see figure 8). Since genuine *ep* interactions will produce particles which must pass through the EMC layer before the HAC cells, these interactions will not be purely hadronic.
- Q^2_{JB} >400 GeV^2
  A lower limit on the measured value of Q^2, using Jacquet-Blondel reconstruction, is required. This is done to restrict the sample to a region where the Jacquet-Blondel estimators give good resolution for the kinematic quantities. The Q^2 distribution is shown in figure 9.
- y_{JB} <0.9
  An upper limit on the measured value of y_{JB} is required (see figure 10). This contributes to rejecting neutral current events.
- Calorimeter spark rejection
  Calorimeter photo-multiplier tubes (PMTs) can suffer from random discharges, which fake energy deposits. These sparks in the calorimeter are characterised by a large imbalance in the energy reported by the two PMTs, for the calorimeter cell. These events are identified by this energy imbalance and rejected.
- Photo-production rejection
  Low Q^2 photo-production events, where the scattered positron is lost down the rear beam pipe, result in events with high transverse momentum, which can also have high E_T. These events are a background to the charged current DIS signal. Low Q^2 photo-production events are identified by their track topology, and rejected.

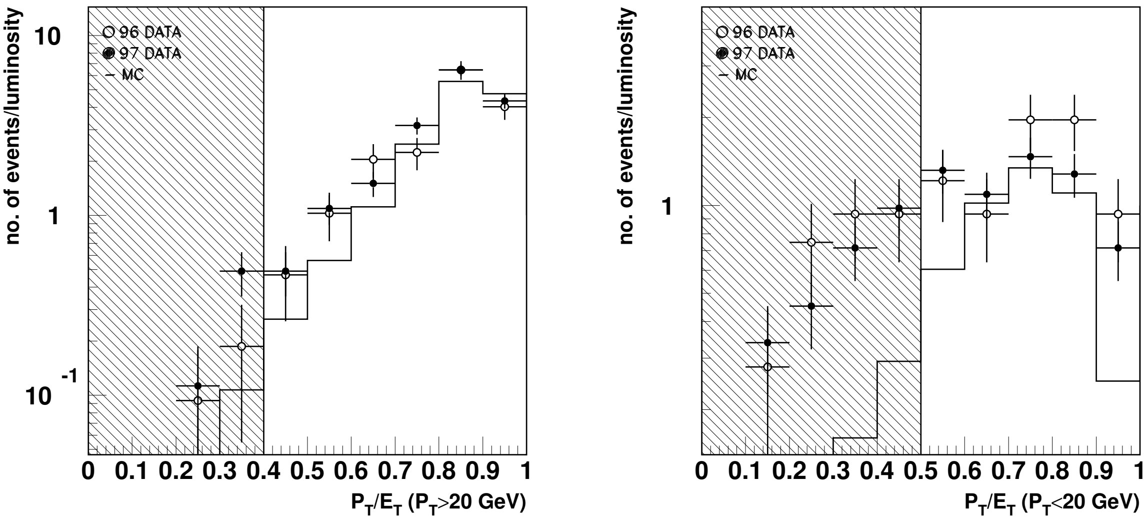

Figure 7: Distribution of P_T/E_T for $P_T > 20$ GeV (left) and $P_T < 20$ GeV (right), for the charged current event sample after all other cuts have been applied. The shaded areas show those events that pass all other cuts but are rejected by the P_T/E_T cuts. In the unshaded regions there is good agreement between data and MC for the $P_T > 20$ GeV case, but an excess of data events in the $P_T < 20$ GeV case.

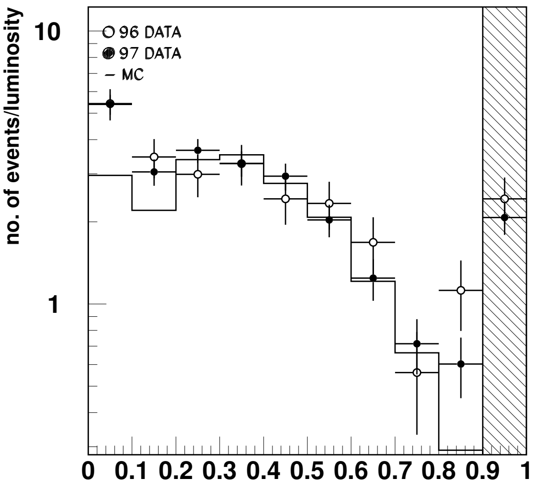

Figure 8: Distribution of E_{BHAC}/E_B, for the charged current event sample after all other cuts have been applied. The shaded area shows those events that pass all other cuts but are rejected by the E_{BHAC}/E_B cut. In the unshaded region there is generally good agreement between data and MC apart from a small excess of data events in the first bin.

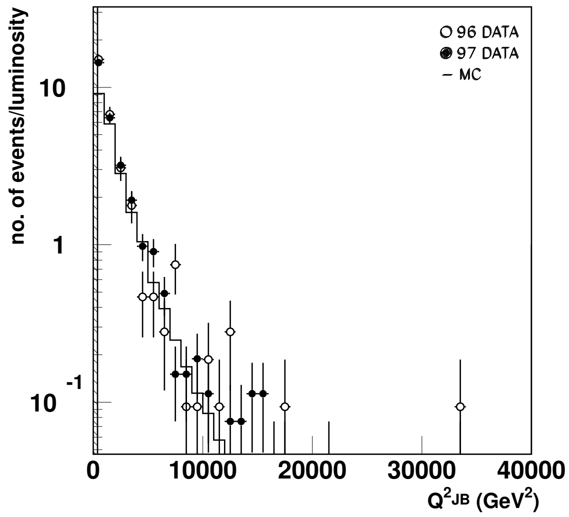

Figure 9: Distribution of Q^2_{JB}, for the charged current event sample after all cuts have been applied. Good agreement between data and MC is observed.

- Neutral current rejection
  Neutral current events with poorly measured electron energy can have high transverse momentum. Neutral current selection cuts are applied, to identify and reject these events.
  - SINISTRA 95 positron
    A positron candidate is required using the SINISTRA 95 [8] program. This uses a neural network to identify the characteristic pattern of energy deposited in the calorimeter by a positron.
    * E'_e >4 GeV
      The energy of the scattered positron candidate is required to be greater than 4 GeV.
    * Prob>0.9
      The probability function of the electron finder must give a high probability of a correctly identified positron.
    * E_{NEAR} <5 GeV
      E_{NEAR} is the energy not associated with the positron candidate in a surrounding η,ϕ cone of 0.8. η is the pseudorapidity, defined as $\eta = -ln\ tan(\theta/2)$. E_{NEAR} is required to be low in order to exclude electromagnetic energy deposits that are inside hadronic jets.
    * D_{CA} < 15 cm (in CTD acceptance)
      If the positron candidate is within the acceptance of the CTD, then it is required to have a matching track that passes within 15 cm of the energy deposited in the calorimeter.
    * P_{T_e} > 20 GeV (forward of CTD acceptance)
      Positron candidates that are forward of the CTD acceptance are required to have at least 20 GeV of transverse momentum. Requiring high transverse momentum distinguishes genuine positrons from hadronic deposits.

Also cosmic muon rejection (using the algorithm ISITAMU [9]), and calorimeter and island timing cuts (see section 5.4) are used to reject non-*ep* interactions. The muon rejection uses the topology of calorimeter energy deeposits to identify and reject cosmic and beam halo muon events. Runs unsuitable for physics analysis, for some reason, such as failure of a detector component, are rejected.

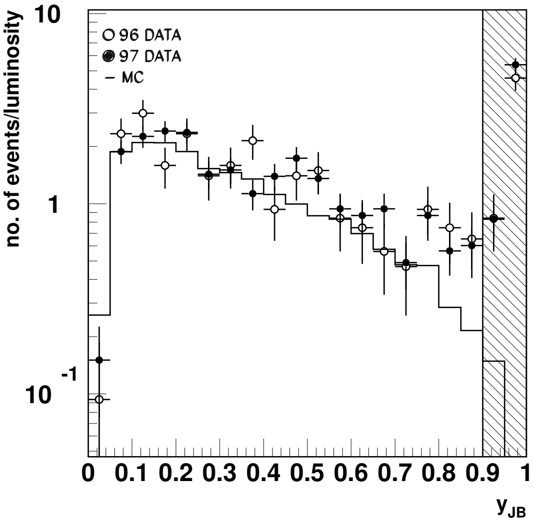

Figure 10: Distribution of y_{JB}, for the charged current event sample after all other cuts have been applied. The shaded area shows those events that pass all other cuts but are rejected by the y_{JB} cut. In the unshaded region there is reasonable agreement between data and MC.

5.3 Neutral current sample

- Trigger requirements
  - First level trigger
    The first level trigger requires an isolated positron candidate in RCAL, and in addition at least one of the following conditions must be satisfied.
    - total EMC energy in RCAL $\geq$ 3.750 GeV
    - total EMC energy in RCAL (excluding the towers adjacent to the beam pipe) $\geq$ 2.032 GeV
    - total energy deposited in the calorimeter > 0.464 GeV

    Also background from proton interactions outside the detector is rejected using timing from up-stream veto counters.
- 35< $E - p_z$ <65
  This cut selects accurately measured neutral current events. These events will have $E - p_z$ of around twice the positron beam energy because of the choice of coordinate system. Also the lower threshold rejects background from photo-production.
- -50cm< Z_{vtx} <50cm
  The z position of the *ep* interaction vertex is required to be within 50cm of the nominal interaction point at z=0 (see figure 11).
- $N_{vtx} \geq 1$
  At least one vertex track is required (see figure 12). A vertex track is defined as a track with P_T >0.2 GeV which passes within 1.5cm of the nominal beam line.
- $N_{vtx} > 0.25(N_{trks}$-20)
  A large fraction of tracks are required to be vertex tracks.
- SINISTRA 95 positron
  A positron candidate is required using SINISTRA 95.
  - 13cm×8cm RCAL box cut
    Events are rejected if the positron candidate is detected close to the RCAL beam pipe. This ensures the positron position and energy can be measured accurately.

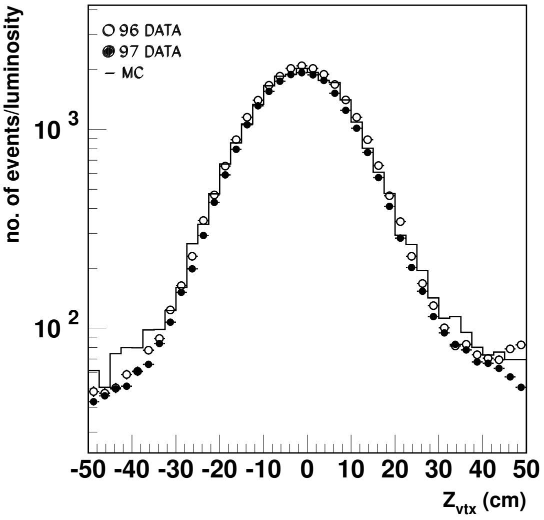

Figure 11: Distribution of the z position of the interaction vertex, for the neutral current event sample after all cuts have been applied. Good agreement is observed between data and MC.

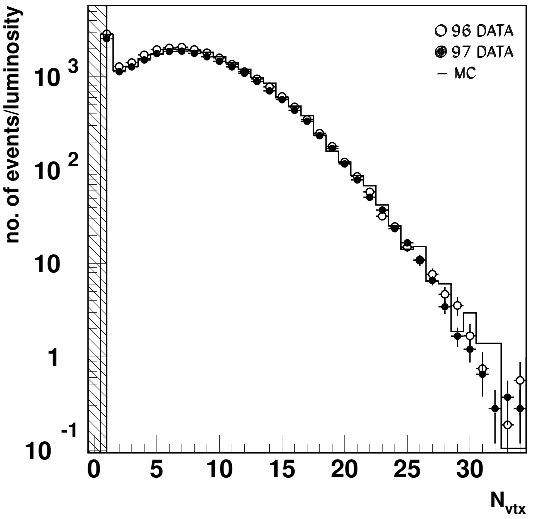

Figure 12: Distribution of vertex track multiplicity, for the neutral current event sample after all other cuts have been applied. The shaded area shows those events that pass all other cuts but are rejected by the vertex track multiplicity cut. In the unshaded region there is good agreement between data and MC.

– E'_e >8 GeV
The energy of the positron candidate is required to be greater than 8 GeV (see figure 13). The energy of the positron is corrected to account for energy loss due to inactive material between the interaction point and the calorimeter (see [10]).

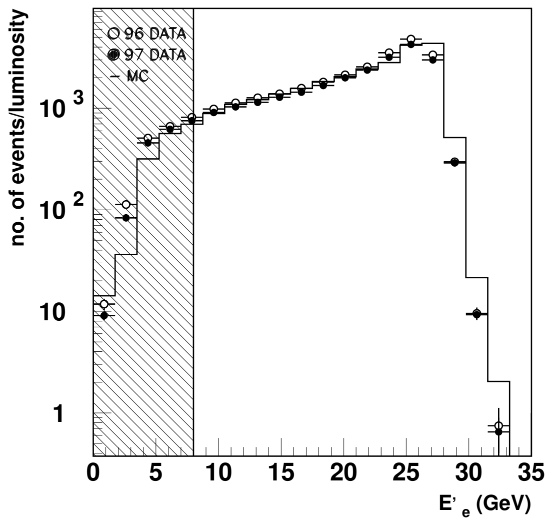

Figure 13: Distribution of scattered positron energy, E'_e, for the neutral current event sample after all other cuts have been applied. The shaded area shows those events that pass all other cuts but are rejected by the E'_e cut. In the unshaded region there is good agreement between data and MC.

– Prob>0.9
The probability function of the electron finder must give a high probability of a correctly identified positron.
– Z_e <-150 cm
The positron is required to be detected in RCAL.
– E_{NEAR} < 5 GeV
The energy not associated with the positron candidate in a surrounding η,ϕ cone of 0.8, E_{NEAR}, is required to be low (see figure 14).

- Calorimeter spark rejection
Events with a calorimeter spark are identified and rejected.
- Q^2_e >20 GeV^2
A lower limit on the measured value of Q^2, using the electron reconstruction method, is required. The Q^2_e distribution is shown in figure 15.

Also muon rejection (ISITAMU), and calorimeter and island timing cuts (see section 5.4) are used to reject non-*ep* interactions. Runs unsuitable for physics analysis are rejected.

5.4 Calorimeter timing cuts

The calorimeter provides high precision timing for each cell. Each calorimeter cell has a local clock, which is offset according to the geometry of the calorimeter. The offsets are chosen such that a particle travelling at the speed of light from the nominal interaction point will strike any cell at the cell's time t=0. The timing is also tied into the HERA bunch crossing time, so that calorimeter timing cuts can be used to reject non-ep interactions and noise. The timing distributions will also be sensitive to the vertex distributions since the

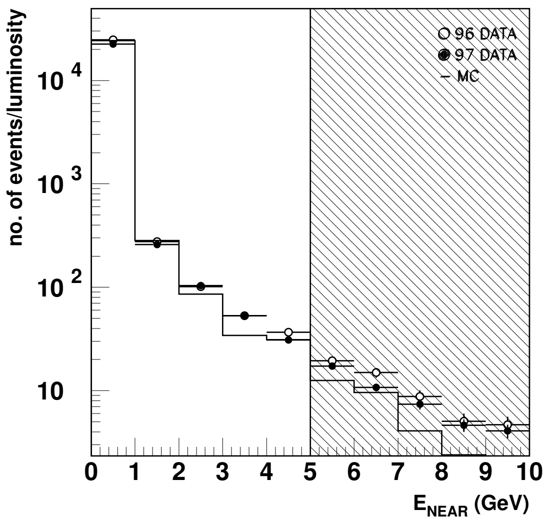

Figure 14: Distribution of E_{NEAR}, the energy not associated with the positron candidate in a surrounding η,ϕ cone of 0.8, for the neutral current event sample after all other cuts have been applied. The shaded area shows those events that pass all other cuts but are rejected by the E_{NEAR} cut. In the unshaded region there is good agreement between data and MC.

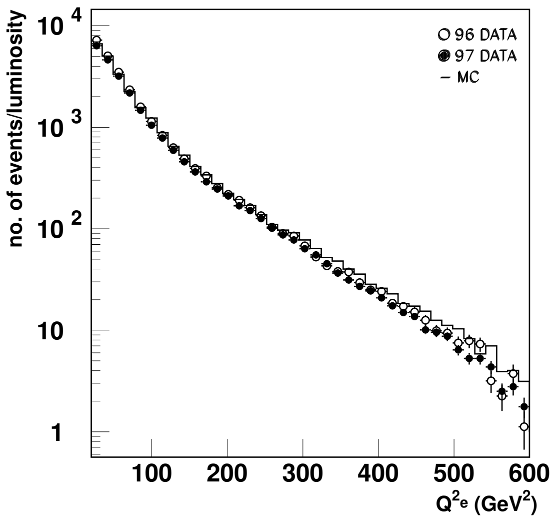

Figure 15: Distribution of Q^2_e, for the neutral current event sample after all cuts have been applied. Good agreement is observed between data and MC.

timing assumes the nominal vertex position.

Calorimeter timign cuts were used to reject events that were not consistant with an interection near the nominal interaction point. Calorimeter timing cuts were applied to the FCAL and RCAL separately, and also to the global calorimeter time, the interval between the FCAL and RCAL times, and the interval between the times for the upper and lower halves of the BCAL. The global calorimeter time is an average of the times from the different sections of the calorimeter. Events were rejected using the timing cuts only if both PMTs for each calorimeter cell were used in the energy calculation. The calorimeter timing cuts used are summarised in table 2.

$\mid T_{FCAL} \mid < 6ns$	$E_{FCAL} > 0.6GeV$
$\mid T_{FCAL} \mid < 5ns$	$E_{FCAL} > 10GeV$
$\mid T_{RCAL} \mid < 6ns$	$E_{RCAL} > 0.6GeV$
$\mid T_{RCAL} \mid < 5ns$	$E_{RCAL} > 10GeV$
$\mid T_{GLOBAL} \mid < 6ns$	$E_{GLOBAL} > 2GeV$
$\mid T_{FCAL} - T_{RCAL} \mid < 6ns$	E_{FCAL} and $E_{RCAL} > 1GeV$
$\mid T_{BCAL}(UP) - T_{BCAL}(DOWN) \mid < 8ns$	$E_{BCAL}(UP)$ and $E_{BCAL}(DOWN) > 1GeV$

Table 2: Summary of calorimeter timing cuts.

In addition cuts based on the timing for calorimeter islands were used. Energy deposits in neighbouring calorimeter cells are combined into energy islands. An energy weighted average of the cell times is assigned to each island. A cut of

$$\mid T_{ISLAND} \mid < 7ns$$

was made on the time of the maximum and minimum time island in each event. These cuts remove cosmic ray events and beam halo muon events, which pass through a large fraction of the calorimeter and therefore have acceptable average times, but deposit some energy at earlier or later times.

6 The charged current trigger

Events are filtered online by a three level trigger system [1].

The first level trigger (FLT) conditions reject background from protons interacting outside the detector using the time measurement of the energy deposits in upstream veto counters and the SRTD[1]. Charged current candidate events are required to satisfy at least one of:

- $P_T \geq 5$ GeV and $E_T \geq 5$ GeV and a good track found in the CTD.
- $P_T \geq 8$ GeV and a good track or very good track found in the CTD.
- $P_T \geq 8$ GeV and at least 10 GeV of energy in FCAL.

The second level trigger uses the measured times of energy deposits in the calorimeter to remove background events for which the timing of the deposits is not consistant with an *ep* interaction from a HERA bunch crossing. Charged current candidate events are accepted if at least one of the following conditions is satisfied.

- $P_T > 6$ GeV and E_T (excluding the two rings of cells closest to the forward beam pipe) > 6 GeV and a good track found in the CTD.
- $P_T > 9$ GeV and P_T (excluding the cells adjacent to the forward beam pipe) > 8 GeV and at least 20 GeV of energy in FCAL.
- $P_T > 9$ GeV and $P_T/\sqrt{E_T} > 2.1$ and at least 80 GeV of energy in FCAL.

[1]The small angle rear tracking detector (SRTD) lies on the front face of RCAL, close to the beam pipe, and is used to correct the energy and position measurments of positrons scattered through small angles relative to the positron beam direction.

The full event information is available to the third level trigger. Tighter timing cuts in addition to algorithms to remove proton interactions with gas in the beam pipe are applied. Charged current candidate events are selected using the requirement:

- $P_T > 8$ GeV

Comparison between data and Monte Carlo for the FLT quantities, evaluated by the charged current trigger is shown in figure 16 for the charged current sample and figure 17 for the neutral current sample. The shaded areas show events that do not pass the charged current trigger requirements.

7 Trigger efficiency

7.1 Calorimeter efficiency

The calorimeter first level trigger (CFLT) evaluates the energy of each event by grouping neighbouring calorimeter cells into trigger towers and summing the energy in the towers. The energy in each trigger tower is approximated in analogue to digital conversion, which results in a discrepancy between the CFLT energy and the offline calorimeter energy where the energy from each individual cell is included. The offline equivalent of each CFLT quantity can be used to plot a turn-on curve for each CFLT cut. The efficiency in each bin of the turn-on curves is the number of events in the offline sample that satisfy the CLFT cut divided by the total number of events in the offline sample. Each turn-on curve can then be fitted to the function:

$$\eta = \frac{1}{2} tanh \left(\frac{x - p_1}{p_2} \right) + \frac{1}{2} \tag{10}$$

where η is the efficiency, and p_1 and p_2 are parameters which represent the position and width of the turn-on curve. The turn-on curves parameterise the efficiency of the CFLT in terms of offline calorimter quantities. Turn-on curves for each of the CFLT cuts in the charged current trigger are shown in figure 18. The turn-on curves for $E_T \geq 5$ GeV and $E_{FCAL} \geq 10$ GeV are well described by the function (10) and show a small shift in the position of the turn-on curves between data and MC. The topology of the netral current events means that the curves for $P_T \geq 5$ GeV and $P_T \geq 8$ GeV have very limited statistics in the range $P_T >\sim 10$ GeV, so the fits use the large number of events at low P_T, and parameterise the turn-on curves poorly. These curves also show a shift in the position of the turn-on curves between data and MC.

7.2 Tracking efficiency

The effect of the tracking vetos in the charged current trigger on data and Monte Carlo is compared. This is done by considering the fraction of all the events that satisfy the neutral current offline selection, that also satisfy the tracking vetos. The neutral current selection is chosen such that it duplicates the charged current selection for quantities that have a large effect on the tracking, such as interaction vertex z position and track topology cuts. Comparison of this fraction between data and Monte Carlo is given in table 3.

Track veto	1996 data	1997 data	MC
Very good track	77.53 ± 0.11	78.27 ± 0.08	74.40 ± 0.13
Good track	95.39 ± 0.06	96.72 ± 0.04	97.85 ± 0.04

Table 3: Values of the tracking efficiency (%), for the neutral current event sample.

7.3 Combined efficiency

The efficiency for each event, η_i, in the charged current sample can be calculated from the parameterised turn-on curves and the tracking veto efficiency. The efficiency is given by the product of the inefficiency of each branch of the charged current FLT for each event:

$$\eta_i = 1 - (1 - \eta_{P_{T1}} \eta_{E_T} \eta_{GT})(1 - \eta_{P_{T2}}(1 - \eta_{FCAL})(1 - (1 - \eta_{GT})(1 - \eta_{VGT}))) \tag{11}$$

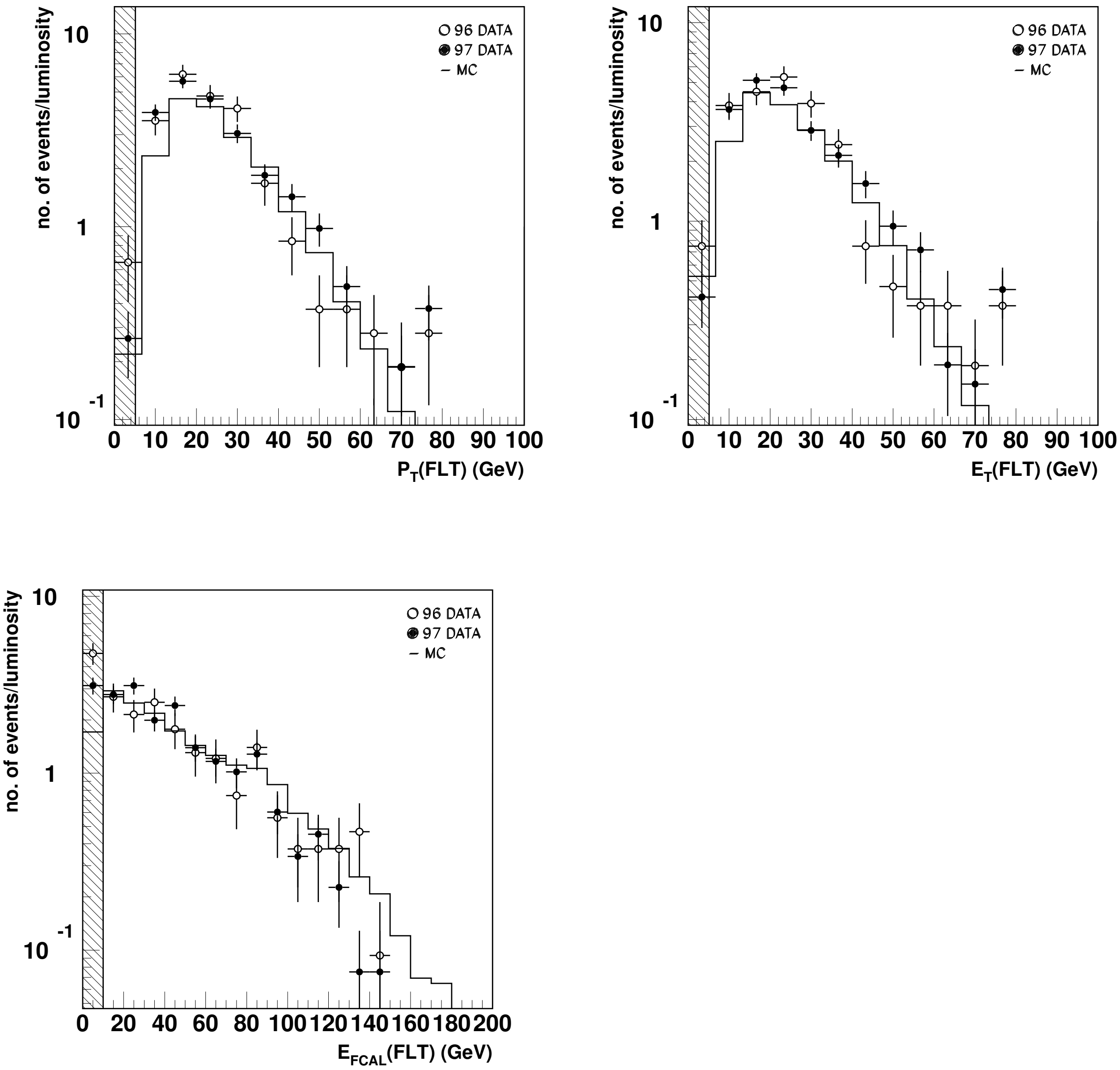

Figure 16: Distributions of the FLT quantities evaluated in the charged current trigger, for the charged current sample.

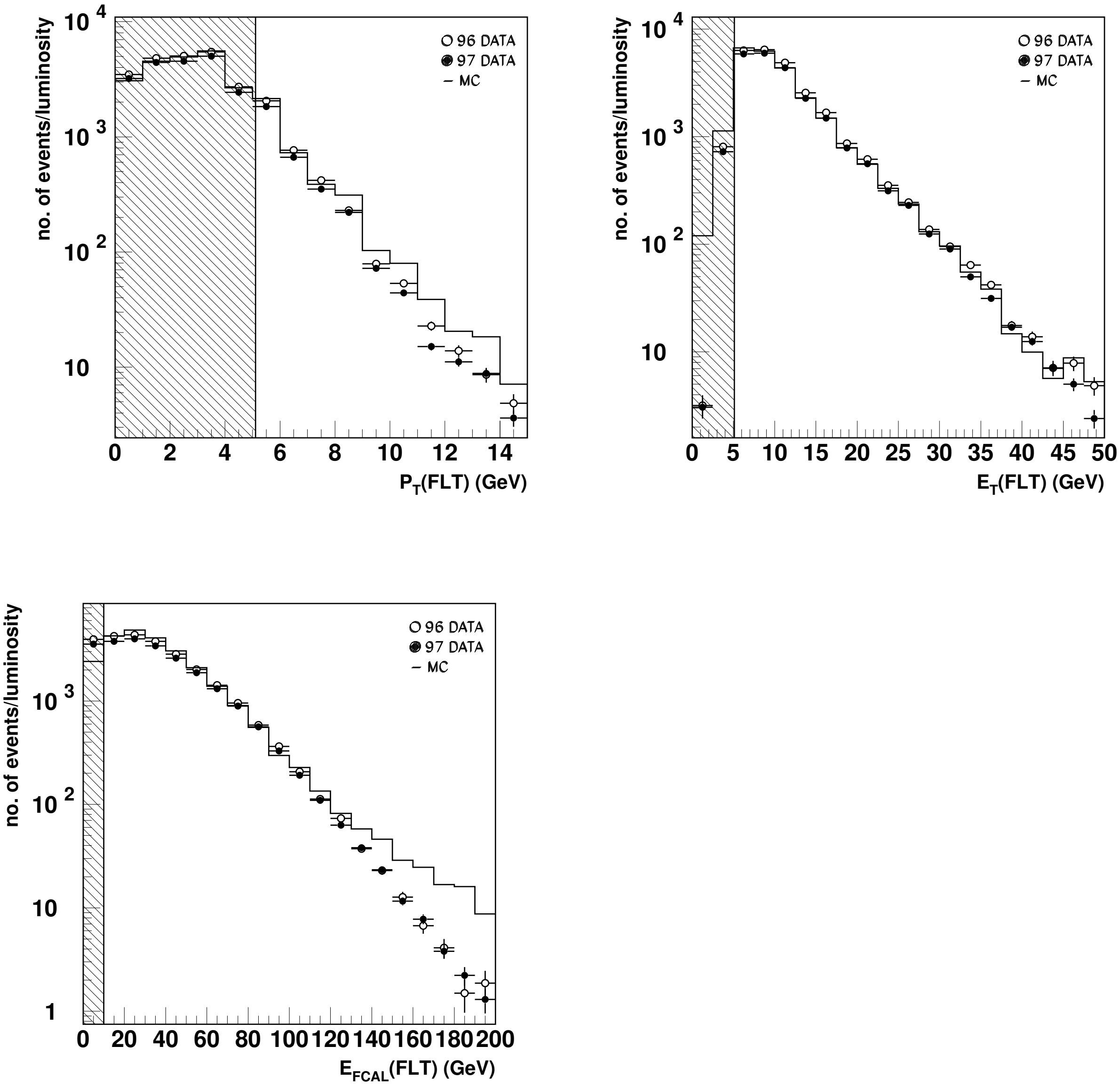

Figure 17: Distributions of the FLT quantities evaluated in the charged current trigger, for the neutral current sample.

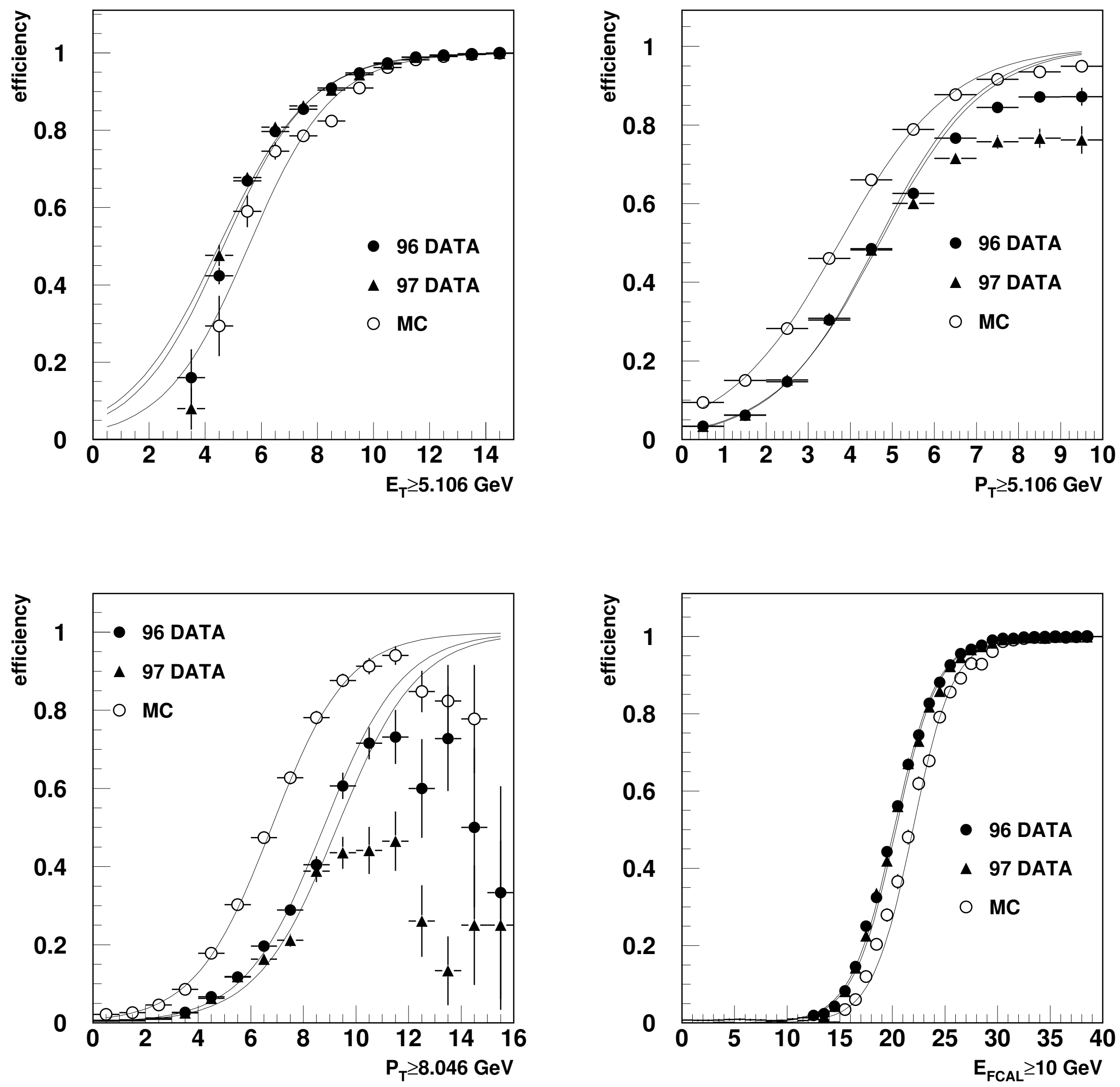

Figure 18: Efficiency turn-on curves for each of the CFLT cuts in the charged current trigger, for the neutral current event sample. The efficiency of each CLFT cut is parameterised in terms of the relavent offline calorimeter quantity.

where $\eta_{P_{T1}}$, $\eta_{P_{T2}}$, η_{E_T} and η_{FCAL} are the efficiencies for each of the CFLT cuts, for each event. η_{GT} and η_{VGT} are the efficiencies for the good track and very good track vetos, and are set to the values given in table 3 for all events.

The efficiencies for each of the events in the charged current sample are then used to calculate the mean efficiency,

$$\bar{\eta} = \frac{1}{N}\sum \eta_i \tag{12}$$

where N is the number of events in the charged current sample.

The errors quoted for these quantities in section 8 are binomial and statistical only.

8 Results

The overall charged current trigger efficiencies are given in table 4.

Event sample	Mean efficiency (%)
1996 data	98.75 ± 0.70
1997 data	99.14 ± 0.37
MC	99.49 ± 0.03

Table 4: Charged current trigger efficiencies, evaluated for data and Monte Carlo.

9 Conclusion

The charged current trigger efficiency has been evaluated for data taken in 1996 and 1997 and also for Monte Carlo. It is found that the difference in trigger efficiency between data and Monte Carlo is $< 1\%$, and within statistical errors. This difference can be used to calculate the contribution from the trigger efficiency to the systematic error on the cross-section. It is planned that the knowledge gained in carrying out this analysis will be used to redefine the charged current trigger for the 1998 run and onwards.

10 Acknowledgements

Thanks to Rod and Gareth for the charged current selection and Jo for help with the neutral current cuts. Thanks also to Ken, Arnie and Jo Edmonds for their advice.

References

[1] ZEUS Collab., The ZEUS Detector, Status Report 1993, DESY 1993.

[2] HERA, A Proposal for a Large Electron-Proton Colliding Beam Facility at DESY, DESY HERA 81-10

[3] F. Jacquet, A. Blondel, Proc. of the study for an *ep* facility for Europe, DESY 79-48 (1979) 391

[4] S. Bentvelsen, J. Engelen, P. Kooijman, Reconstruction of (x, Q^2) and extraction of structure functions in neutral current scattering at HERA, In Proc. of the HERA Workshop Vol. 1, (1991) 23

[5] K. Charchula, G.A. Schuler and H. Spiesberger, DJANGO6 2.4, Comp. Phys. Comm. **81** (1994).

[6] G. Ingelman, A. Edin and J. Rathsman, LEPTO 6.5, Comp. Phys. Comm. **101** (1997).

[7] H. Spiesberger, HERACLES 4.5.2, unpublished program manual (1993)

[8] H. Abramowicz, A. Caldwell, R. Sinkus, Nucl. Inst. Meth., **A365** (1995)

[9] H. Abramowicz, ISITAMU algorithm, ZEUS software.

[10] J. E. Cole, A Study of Positron Energy Correction in 1995 DIS Data using the SRTD, ZEUS-Note 98-022